

Effects of annealing on amorphous Gd_xSi_{1-x} near the metal-insulator transition

E. Guillotel

Department of Physics, University of California, Berkeley, California 94720

L. Zeng^{a)}

Material Science Program, University of California San Diego, La Jolla, California 92093

E. Helgren and F. Hellman

Department of Physics, University of California, Berkeley, California 94720

R. Islam and David J. Smith

Center for Solid State Science, Arizona State University, Tempe, Arizona 85287 and Department of Physics, Arizona State University, Tempe, Arizona 85287

(Received 30 August 2006; accepted 3 November 2006; published online 19 January 2007)

Annealing of amorphous Gd–Si films produces large changes in magnetic and magnetotransport properties. The materials have spin-glass freezing and enormous negative magnetoresistance (MR) in the unannealed state but show drastically reduced MR and magnetization on annealing. These changes can be explained by high resolution transmission electron micrographs and energy-dispersive x-ray analysis which show the appearance of nanocrystalline clusters of GdSi and GdSi₂ in an amorphous background. A comparison with the nonmagnetic analog Y–Si shows similar modification of electrical properties. © 2007 American Institute of Physics.

[DOI: [10.1063/1.2426921](https://doi.org/10.1063/1.2426921)]

INTRODUCTION

Amorphous semiconductors are of great interest for their electronic and optical properties. The introduction of transition metal elements such as Nb, Mo, or Fe into amorphous semiconductors such as Si leads to increased conductivity and a metal-insulator transition (MIT) for metal concentrations around 10–15 at. %, where insulators are defined as having zero conductivity with an activated temperature dependence in the limit as T goes to zero and metals have finite, nonzero conductivity, and power law dependence in the same limit.¹ Introduction of the magnetic element Gd has similarly been shown to lead to a MIT for amorphous Gd–Si alloys (a -Gd _{x} Si _{$1-x$}) with $x=14.0$ at. % Gd;^{2–6} this alloy also shows dramatic magnetic and magnetotransport effects, including enormous (many orders of magnitude) negative magnetoresistance^{3,4} (MR) below a characteristic temperature T^* .⁶ Amorphous Si alloys have been studied after thermal treatment and show the formation of nanometer-sized grains.^{7–10} In a recent paper,¹¹ we showed that annealed a -Nb–Si develops Nb-rich clusters within a Nb-depleted amorphous matrix, causing the resistivity to increase dramatically and leading to improvements in the technological use of a -Nb–Si resistance thermometers. The results for a -Nb–Si suggested the possibility that small paramagnetic Gd clusters in an amorphous Gd-depleted matrix could lead to enhanced response to smaller magnetic fields and hence higher MR, perhaps also accompanied by an increase in T^* . A study of the effect of annealing on the structure, magnetic, and magnetotransport properties of a -Gd _{x} Si _{$1-x$} alloys near the MIT and the nonmagnetic analog a -Y _{x} Si _{$1-x$} was therefore

undertaken. Annealing was found to cause nanocrystalline clusters to develop, rather than small composition fluctuations as seen in a -Nb–Si, with significant effects on the electrical conductivity (σ_{dc}), MR, magnetization, and magnetic susceptibility.

EXPERIMENT

Samples were made by electron beam coevaporation under ultrahigh vacuum conditions from separately controlled Si and Gd or Y sources onto amorphous silicon nitride-coated Si substrates held near room temperature. Thickness was measured with a Dektak profilometer. A typical annealing profile was 30 s to reach the desired annealing temperature T_a , followed by 1 min at T_a , after which the heater was turned off and the temperature relaxed approximately exponentially to room temperature (~ 5 min to reach 50 °C). Temperature during annealing was measured with a thermocouple inserted inside the sample plate. Error bars on σ_{dc} and T are $\sim 5\%$. Gd and Y compositions were determined by Rutherford backscattering (RBS). Samples were annealed using a rapid thermal annealing (RTA) system in flowing forming gas (5% H₂ in N₂ gas, used to capture O₂). Magnetic properties were measured in a Quantum Design MPMS. Conductivity as a function of temperature T and magnetic field H , $\sigma_{dc}(T, H)$, was measured from 4 to 298 K and 0–7 T using samples lithographically patterned for four-point-probe measurements.

RESULTS

Figure 1 shows σ_{dc} vs T for two samples on the metallic side of the MIT (14.5 at. % Gd and 14.4 at. % Y, referred to as G0 and Y, respectively) after annealing at the temperatures

^{a)}Electronic mail: li_zeng@berkeley.edu

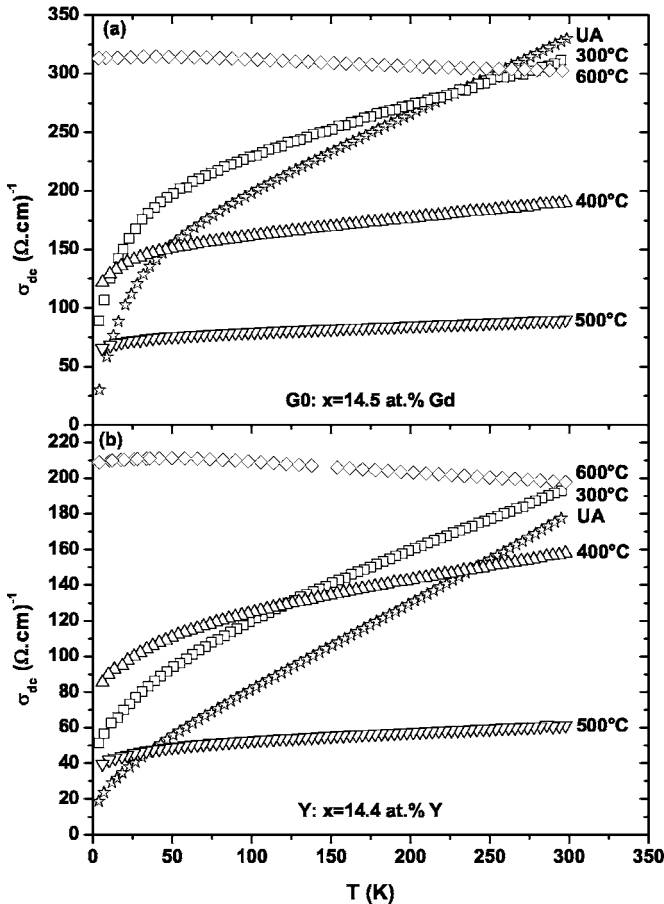


FIG. 1. Conductivity $\sigma_{dc}(T)$ for (a) $a\text{-Gd}_{14.5}\text{Si}_{85.5}$ (G0) and (b) $a\text{-Y}_{14.4}\text{Si}_{85.6}$ (Y) (both on the metallic side of the MIT) in the unannealed (UA) state and for various annealing temperatures T_a up to 600 °C.

T_a shown. The data show three separate annealing regimes. For low T_a (up to 300 °C for sample G0 Fig. 1(a) and up to 400 °C for sample Y [Fig. 1(b)], the samples become more conducting. For higher T_a , σ_{dc} decreases at all T . Finally, at $T_a=600$ °C, samples become fully metallic, with very low but nearly temperature-independent conductivity. The dependence of σ_{dc} on T_a is thus different at high and low measurement temperature T , which suggests a modification in the mode of conduction, seen for both the magnetic and non-magnetic alloys. Especially at low measurement T , the changes in σ_{dc} with annealing are not monotonic, while at higher T , after an increase of σ_{dc} for $T_a=300$ or 400 °C, σ continuously decreases with increasing T_a up to $T_a=500$ °C. Annealing at ~ 400 °C thus appears to produce significant changes in the properties of these alloys.

Figure 2 shows the evolution of $\sigma_{dc}(T)$ with T_a for two Gd–Si samples on the insulating side of the MIT, G1, and G2 with $x=12.5$ and 10 at. %, respectively. The same changes with T_a as previously discussed are also observed here, leading to the conclusion that composition plays no significant role in the effects of annealing over this composition range. Most significantly, both G1 and G2 become metallic at the highest annealing temperature, with very low but nearly temperature-independent $\sigma_{dc}(T)$ when annealed at 500 and 600 °C, respectively, shown most clearly in the insets of Fig. 2. For all samples (G0–G2, Y), at low measurement tempera-

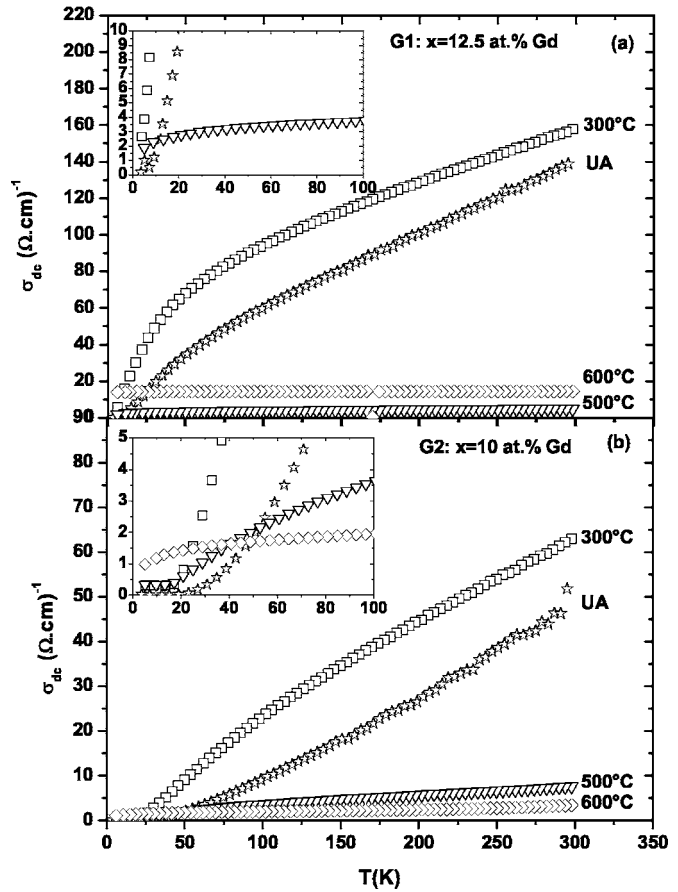


FIG. 2. Conductivity $\sigma_{dc}(T)$ for (a) $a\text{-Gd}_{12.5}\text{Si}_{87.5}$ (G1) and (b) $a\text{-Gd}_{10}\text{Si}_{90}$ (G2), both on the insulating side of the MIT in the UA state and for various annealing temperatures T_a up to 600 °C. Insets: expanded low T , low σ scale showing metallic σ for $T_a=500$ and 600 °C, respectively (temperature independent with finite σ at $T=0$).

ture T , σ_{dc} is higher for $T_a=600$ °C than 500 °C. The increase, however, decreases with decreasing metallic concentration, and for G2, with the lowest Gd concentration, the two data sets (σ_{dc} for $T_a=600$ °C and $T_a=500$ °C) cross.

Figure 3 shows the dependence of the magnetoconductance (MG), $\sigma_{dc}(H)$, at $T=2$ K on annealing for sample G0. MG is defined as $([\sigma(70 \text{ kOe}) - \sigma(0 \text{ kOe})] / \sigma(0 \text{ kOe}))$, mathematically equal to the negative of the magnetoresistance ($-\text{MR}$), as usually defined $([\rho(70 \text{ kOe}) - \rho(0 \text{ kOe})] / \rho(70 \text{ kOe}))$. Previous extensive studies of MG of Gd–Si alloys have shown σ (and ρ) to be independent of field direction, both relative to film plane and relative to current direction.³ In the present experiment, the field was applied in the plane of the film, parallel to the direction of current flow. For the unannealed sample, MG is about 180% at 2 K; this number is typical for samples on the metallic side of the MI transition. Like σ_{dc} itself, MG is changed negligibly by annealing at 200 °C. For higher T_a , the MG drops substantially (38%, 4%, and 1% for $T_a=300$, 400, and 500 °C, respectively). Figure 4 shows MG as a function of measurement temperature. MG decreases with increasing T , for all T_a , and vanishes above 50 K.

The effects of annealing on the magnetic properties are shown in Figs. 5 and 6 for various T_a . Figure 5 shows magnetization versus field, $M(H)$, at 2 K. All data, including the

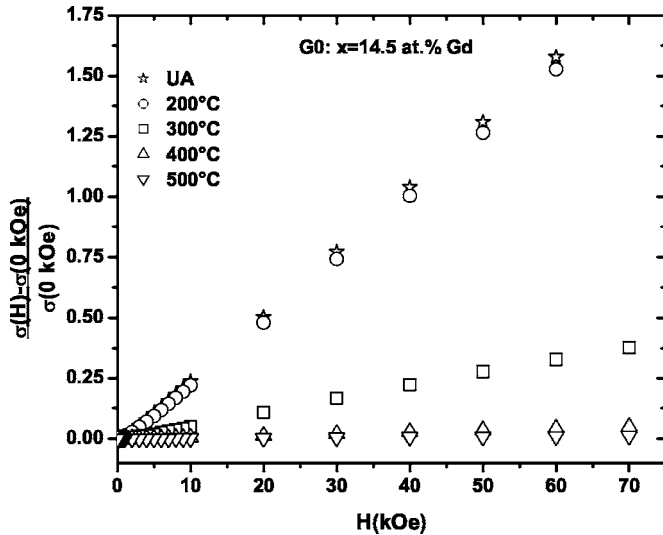


FIG. 3. Magnetoconductance (MG) vs H at $T=2$ K in the UA state and for various annealing temperatures T_a to 500 °C. $MG(H)=[\sigma(H)-\sigma(0)]/\sigma(0)$ ($=-\text{MR}$ as usually defined) for G0 (14.5 at. % Gd).

unannealed (UA) sample, are significantly below the Brillouin function for noninteracting Gd moments, as previously found,¹² indicative of antiferromagnetic Gd–Gd interactions and consistent with the spin-glass freezing discussed in that study. Annealing at 200 or 300 °C produces no change in $M(H)$, but annealing at higher temperature (400–600 °C) reduce $M(H)$ even further below the noninteracting Brillouin function limit. Figure 6 presents the magnetic susceptibility versus temperature, $\chi_{dc}(T)$, defined as M/H , with $H=500$ Oe (M is experimentally observed to be linear in H up to 500 Oe). Data are taken on heating after cooling in zero field to 2 K (the zero field cooled (ZFC) state). The sample unannealed and after annealing at T_a up to 300 °C show a peak characteristic of the spin-glass freezing previously seen for Gd–Si in the UA state.¹² The freezing temperature (determined from the split between ZFC and FC data) increases from 6 to 6.5 K and the magnitude of χ_{dc} decreases on an-

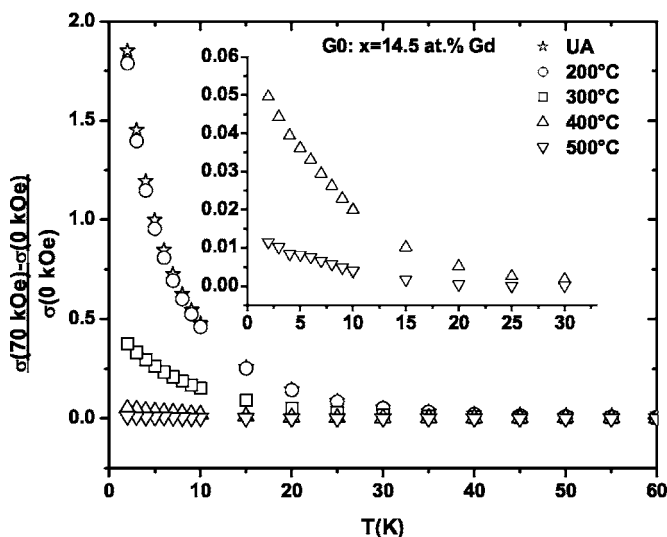


FIG. 4. MG vs T for $H=70$ kOe $=[\sigma(70$ kOe) $-\sigma(0)]/\sigma(0)$ ($=-\text{MR}$) in the UA state and for various annealing temperatures T_a up to 500 °C for G0 (14.5 at. % Gd). Inset: expanded scales for $T_a=400$ and 500 °C.

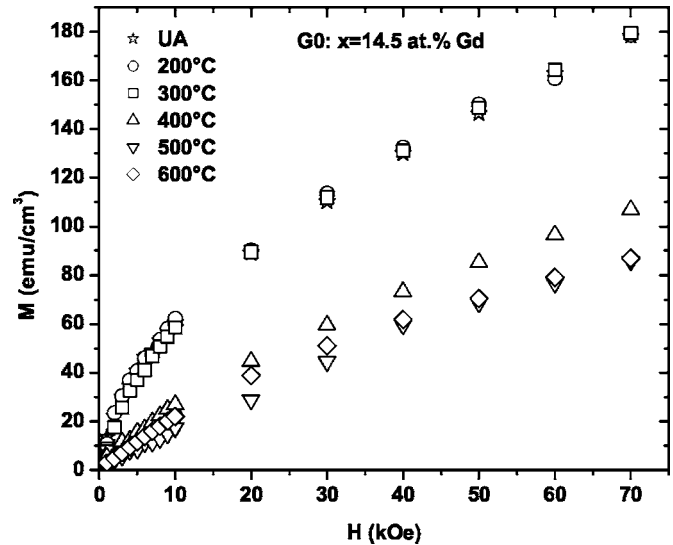


FIG. 5. $M(H)$ for sample G0 (14.5 at. % Gd) measured at $T=2$ K in the UA state and for various annealing temperatures T_a up to 600 °C as shown.

nealing up to 300 °C. For higher T_a , χ_{dc} shows no peak, to the lowest measurement temperature (2 K), and a large decrease in magnitude of $\chi_{dc}(T)$ with increasing T_a . These data are evidence of increasingly large antiferromagnetic interactions which strongly limit the field response.

High resolution cross-section transmission electron microscopy (HR-XTEM) observations of sample G0 annealed at different T_a are shown in Fig. 7. For $T_a=250$ °C, as for the UA sample, the system is amorphous and shows columnar microstructure which is quite common for vapor-deposited amorphous materials. For $T_a=400$ °C, electron micrographs show the formation of clusters of fringes associated with randomly distributed nanocrystallites (examples are circled); the lattice spacings of these fringes indicate that the phase formed is orthorhombic GdSi₂. For $T_a=500$ °C, fringe clusters are bigger and the spacing for at least one

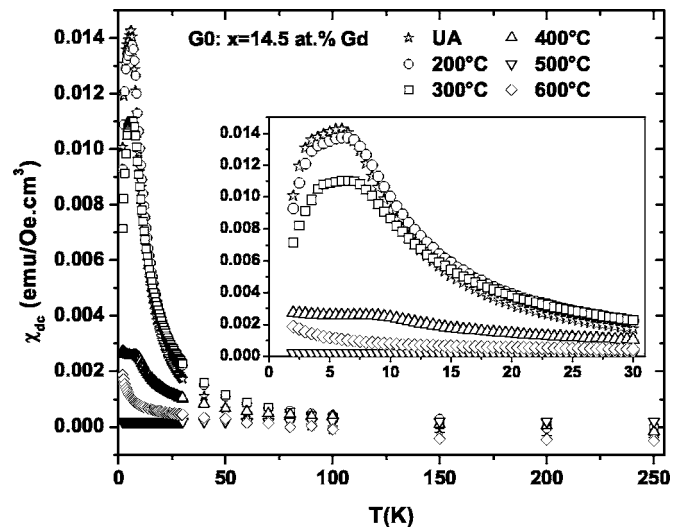


FIG. 6. Magnetic susceptibility $\chi(T)$ for sample G0 (14.5 at. % Gd) measured in 500 Oe on heating after zero field cooled (ZFC) for various annealing temperatures T_a up to 600 °C. $\chi(T)$ in the field cooled (FC) state is identical to the ZFC data above a freezing temperature which is approximately the peak in the ZFC data shown.

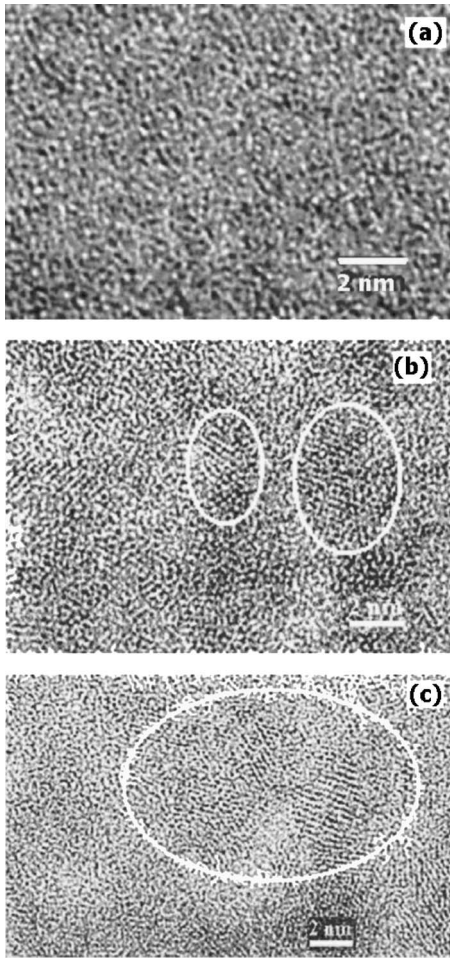


FIG. 7. High resolution cross section transmission electron microscopy (HR-XTEM) of $a\text{-Gd}_{14.5}\text{Si}_{85.5}$ annealed at (a) 200 °C, (b) 400 °C, and (c) 500 °C. The circles show areas of nanocrystalline fringes. Lattice spacings are counted directly from such images and matched to known lattice spacings for Gd–Si compounds.

grain suggests orthorhombic GdSi (other grains can be indexed with either GdSi or GdSi₂). Since the overall composition of the film is 14.5 at. % Gd, for which equilibrium should be a mixture of GdSi₂ and Si, formation of equiatomic GdSi is not expected, particularly since the equilibrium GdSi₂ has already been found after annealing at 400 °C. X-ray diffraction shows evidence of GdSi₂ for $T_a=500$ and 600 °C, with a grain size of ~ 20 nm (based on peak width), plus a suggestion of a broad peak which could be associated with very small GdSi nanocrystallites (~ 2 nm). For $T_a=400$ °C, x-ray diffraction shows no clear peaks. A broad peak near the limit of resolution is consistent with the GdSi₂ nanocrystallite clusters seen in HRTEM images (sizes range from 2 to 5 nm). Figure 8 shows an annular-dark-field (ADF) image and energy-dispersive analysis (EDX) for the sample annealed at $T_a=500$ °C. The bright and dark regions in the ADF image correspond to Gd-rich (high Z) and Gd-poor (low Z) parts of the sample, as confirmed by quantitative Gd and Si EDX profiles taken along the line shown in Fig. 8(a). In contrast, $a\text{-Nb}_x\text{Si}_{1-x}$ films annealed under identical conditions remained amorphous, with very small precursor Nb-rich crystallites. The source of this structural difference is not obvious, since phase dia-

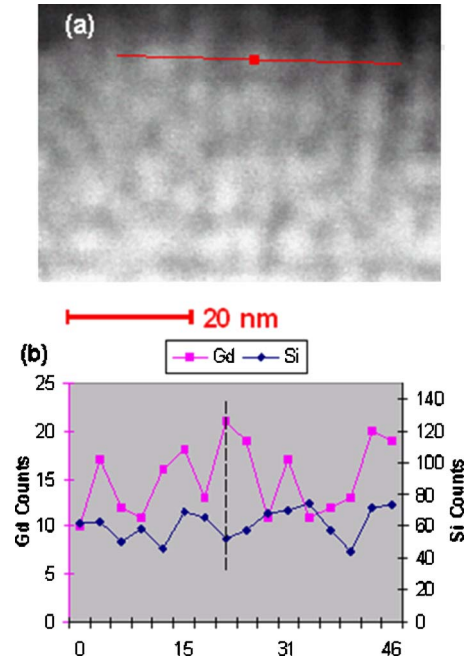


FIG. 8. (Color online) (a) Annular dark field (ADF) image of $a\text{-Gd}_{14.5}\text{Si}_{85.5}$ annealed at 500 °C. (b) Energy-dispersive X-ray (EDX) spectrum profile showing Gd and Si counts along the line shown in (a). Brighter regions in (a) correspond to Gd-rich (high Z) regions in (b), darker ones correspond to Gd-depleted (low Z) regions.

grams and melting temperatures are similar for Si-rich Gd–Si and Nb–Si, differing significantly only in the melting temperatures of pure Gd and pure Nb.

DISCUSSION

The precipitation of Gd-rich crystalline phases with increasing T_a explains the modification of electrical and magnetic properties of the $a\text{-Gd–Si}$ films. At low T_a (up to 300 °C), there is no sign of significant crystallinity. The lack of change in magnetic properties and small increase in conductivity at all measured T are presumably due to a slight increase in density or local relaxation of the amorphous structure, not visible in the HR-XTEM images. At higher T_a (400 or 500 °C) Gd-rich (GdSi and GdSi₂) nanocrystalline clusters develop. These crystalline phases are metallic and antiferromagnetic.^{13–15} Their precipitation causes depletion of Gd from the surrounding Si matrix, leading to a complicated conductivity path which consists of small metallic antiferromagnetic “drops” in a largely insulating amorphous matrix. Increased T_a causes increasingly large metallic clusters to form, creating a percolating metallic path through the sample, and causing metallic behavior with a temperature-independent conductivity whose magnitude decreases with decreasing overall metal concentration (Gd or Y). Although it is unclear *why* GdSi would form for $T_a=500$ °C, the conductivity is consistent with this HR-XTEM result, in that the drop in $\sigma_{dc}(T)$ for $T_a=400$ to 500 °C [seen in Figs. 1(a) and 1(b)] is associated with a smaller volume fraction of GdSi than GdSi₂ (because overall Gd content must be conserved). The vanishing of MR for $T_a \geq 400$ °C is due to reduced $M(H)$, indicating reduced alignment of Gd with field, and the lack of MR expected from conduction dominated by a per-

colating metal path; previous studies showed that polycrystalline GdSi_2 has a small and *positive* MR.^{16,17}

CONCLUSIONS

In summary, annealing has large effects on the properties of $a\text{-Gd}_x\text{Si}_{1-x}$ thin films. For T_a up to 300 °C, there is no significant change in the structure or in any properties. For $T_a > 300$ °C, the samples exhibit complex temperature-dependent conductivity, resulting finally (at $T_a = 600$ °C) in metallic behavior (nearly constant albeit low conductivity), unlike what was seen previously in $a\text{-Nb}_x\text{Si}_{1-x}$. For higher annealing temperatures, MR vanishes and the magnetization and magnetic susceptibility strongly decrease. Structural analysis shows that different phases of crystallized $\text{Gd}_x\text{Si}_{1-x}$ precipitate with annealing explaining these changes in electrical and magnetic properties.

ACKNOWLEDGMENTS

We thank Robert Culbertson for assistance with RBS and gratefully acknowledge the use of facilities in the John M. Cowley Center for High Resolution Electron Microscopy at Arizona State University. This research was supported by NSF DMR-0203907 and 0505524.

- ¹P. A. Lee and T. V. Ramakrishnan, *Rev. Mod. Phys.* **57**, 287 (1985).
- ²J. H. Castilho, I. Chambouleyron, F. C. Marques, C. Rettori, and F. Alvarez, *Phys. Rev. B* **43**, 8946 (1991).
- ³F. Hellman, M. Q. Tran, A. E. Gebala, E. M. Wilcox, and R. C. Dynes, *Phys. Rev. Lett.* **77**, 4652 (1996).
- ⁴P. Xiong, B. L. Zink, S. I. Applebaum, F. Hellman, and R. C. Dynes, *Phys. Rev. B* **59**, R3929 (1999).
- ⁵W. Teizer, F. Hellman, and R. C. Dynes, *Phys. Rev. Lett.* **85**, 848 (2000).
- ⁶E. Helgren, J. J. Cherry, L. Zeng, and F. Hellman, *Phys. Rev. B* **71**, 113203 (2005).
- ⁷A. Csik, G. Erdélyi, G. A. Langer, L. Daróczy, D. L. Beke, J. Nyéki, and Z. Erdélyi, *Vacuum* **80**, 168 (2005).
- ⁸G. Radnoczi, A. Robertsson, H. T. G. Hentzell, S. F. Gong, and M.-A. Hasan, *J. Appl. Phys.* **69**, 6394 (1991).
- ⁹J. R. A. Carlsson, J.-E. Sundgren, L. D. Madsen, X.-H. Li, and H. T. G. Hentzell, *Thin Solid Films* **300**, 51 (1997).
- ¹⁰C. T. M. Ribeiro, M. S. Li, and A. R. Zanatta, *J. Appl. Phys.* **96**, 1068 (2004).
- ¹¹D. Querlioz, E. Helgren, D. R. Queen, F. Hellman, R. Islam, and D. J. Smith, *Appl. Phys. Lett.* **87**, 221901 (2005).
- ¹²F. Hellman, D. R. Queen, R. M. Potok, and B. L. Zink, *Phys. Rev. Lett.* **84**, 5411 (2000).
- ¹³K. Sekizawa and K. Yasuköchi, *J. Phys. Soc. Jpn.* **21**, 274 (1966).
- ¹⁴K. Yaguchi, *J. Phys. Soc. Jpn.* **21**, 405A (1966).
- ¹⁵E. V. Ganapathy, K. Kugimiya, H. Steinfink, and D. I. Tchernev, *J. Less-Common Met.* **44**, 245 (1976).
- ¹⁶C. Boragno, M. R. Bonansinga, and F. Nava, *Solid State Commun.* **92**, 515 (1994).
- ¹⁷S. Labroo and N. Ali, *J. Appl. Phys.* **67**, 4811 (1990).